# Calcium-Looping performance of biomineralised $CaCO_3$ for $CO_2$ capture and thermochemical energy storage

*J. Arcenegui-Troya *,[1] P. E. Sánchez-Jiménez*,[1] A. Perejón,[2,1]*

*J. M. Valverde,[3] R. Chacartegui,[4] and L. A. Pérez-Maqueda[1]*

*[1] Instituto de Ciencia de Materiales de Sevilla, C. S. I. C.-Universidad de Sevilla,*

*C. Américo Vespucio n° 49, 41092 Sevilla, Spain*

*[2] Departamento de Química Inorgánica, Facultad de Química, Universidad de Sevilla, Sevilla, Spain*

*[3] Departamento de Electrónica y Electromagnetismo, Facultad de Física, Universidad de Sevilla,*

*Avenida Reina Mercedes s/n, Sevilla, Spain*

*[4] Departamento de Ingeniería Energética, Escuela Técnica Superior de Ingeniería, Universidad de Sevilla, Camino de los descubrimientos s/n, 41092 Sevilla, Spain*

*(Dated: 23/05/2019)*

***Abstract***

The commercial deployment of calcium looping (CaL) based technologies relies on the availability of non-toxic, widely available and cheap $CaCO_3$ rich materials. Biomineralised $CaCO_3$ from wastes amply fulfil the aforementioned requirements. In the present work, we study the performance of eggshell and snail shell from food waste as CaO precursors for CaL applications. The results obtained in the multicycle calcination/carbonation tests carried out under realistic conditions suggest the feasible use of these waste materials in CaL technology. The multicyclic conversion exhibited by biomineralized $CaCO_3$ was comparable to that demonstrated by limestone, which is a commonly proposed material for CaL applications. In addition, the temperature needed to completely calcine biomineralized $CaCO_3$ in short residence times, as required in practice, is lower than that required to fully calcine limestone, which would mitigate the energy cost of the technology.

*Authors to whom correspondence should be addressed: jjarcenegui@icmse.csic.es, pedro.enrique@icmse.csic.es

## 1. INTRODUCTION

In 2019 36.8 billion metric tons of $CO_2$ were released into the atmosphere because of industrial activities and the combustion of fossil fuels. These emissions are key contributors to global warming. It is estimated that due to the anthropogenic greenhouse gas emissions, the global temperature has already increased by around 1.5 $^oC$ since the industrial revolution [1]. This evidence urges global coordination to reduce CO2 emissions drastically. In this sense, the calcium looping (CaL) process has aroused remarkable interest as a promising technology for reducing $CO_2$ emissions in post-combustion gases [2, 3]. Promising results achieved in pilot-scale tests [4] prove that this technology should be considered as a potential avenue to reduce emissions from highly polluting industries [5].

In the proposed CaL scheme for $CO_2$ capture, the post-combustion gas mixture, containing a low concentration of $CO_2$ (typically 15 %vol), is directed to a fluidised bed reactor where it reacts with solid CaO particles to form $CaCO_3$ at about 650 $^oC$. After carbonation, the carbonated particles are driven into a calciner reactor, where decarbonation takes place during calcination at temperatures around 950 $^oC$ in a $CO_2$ rich atmosphere (around 70 %vol) [3]. Thus, $CO_2$ is released from the calciner in a high purity stream to be compressed and stored, whereas the regenerated CaO particles can be reused in a new cycle [6]. During calcination at high temperatures in a $CO_2$ enriched environment, CaO particles are prone to severe sintering [7, 8]. The strong sintering entails a significant reduction of the active surface that is readily available for carbonation. As a consequence, the maximum CaO conversion attainable at each carbonation stage progressively decreases with the repeating cycles. Sintering-induced CaO deactivation is one of the main limitations of its use for $CO_2$ capture [9, 10].

Recently, the reversible reaction between CaO and $CO_2$ has also been proposed as a thermochemical energy storage system (TCES) for tower-based concentrating solar power (CSP) plants. This solution would overcome the intermittence of direct solar radiation and facilitate power dispatchability of CSP plants [11, 12]. The concept has been extensively explored since Flamant et al. analysed the solar-driven decomposition of $CaCO_3$ for the first time in 1980 [13]. This way, direct solar radiation is used to drive the endothermic decarbonation reaction. The products of the reaction are stored separately and brought together to drive the exothermic carbonation reaction whenever an energy supply is required. Importantly, operation conditions for TCES differ from those suited for $CO_2$ capture. Thus, calcination for TCES could be carried out in inert gas at a relatively low temperature of about 700 $^oC$, while carbonation would be performed in pure $CO_2$ at about 850 $^oC$ [11]. Nevertheless, the problem of incomplete CaO conversion and progressive deactivation remains. It has been observed that under these operation conditions that a $CaCO_3$ blocking layer forms on the particles' surface during the carbonation stage, thereby hindering the percolation of $CO_2$ to the unreacted inner core of the particle [14]. Pore plugging is, in this case, the main limiting mechanism for carbonation.

In order to overcome the issues of incomplete conversion and CaO deactivation, several possible solutions have been explored. Many involve sophisticated sorbent-engineering procedures that are hardly applicable at large scale in commercial plants. The most cost-effective methods involve thermal or mechanical pretreatments or the inclusion of low-cost additives [15]. While different materials have been proposed as CaO precursors, natural limestone remains the most commonly used in pilot tests due to its abundance and low cost [16–18]. Calcium-rich materials, which are affordable, widely available and that require little or no special treatments, are essential for the large-scale deployment of CaL applications, both for $CO_2$ capture and TCES. The deactivation of the sorbent implies its periodic renewal. Its cost is an essential factor to be considered for the efficiency of the process. Thus, the use of materials derived from waste, such as eggshell, becomes attractive [19, 20]. The case of the eggshell is especially compelling. Globally, 80 million tonnes of eggs were produced in 2017 [21]. Eggshell represents approximately 11 % of the entire egg mass. Thus around 8.8 million tonnes of eggshell were thrown away. To put this in perspective, assuming an admittedly optimistic full CaO conversion, the employment of such amounts of this by-product could have resulted in the capture of 3.9 million tonnes of $CO_2$ from the atmosphere in just one single calcination/carbonation cycle. Similarly, according to the Food and Agriculture Organization of the United Nations, 18 thousand tonnes of snails (land snails) were consumed in 2017, which means that approximately 6 thousand tonnes of snail shell were wasted that same year [21].

Both eggshell and snail shell consist mostly of $CaCO_3$ and could, thereby, be used as CaO precursors. This use would provide a useful outlet for a by-product that otherwise would be wasted. Previous works have explored the feasibility of using biomineralised $CaCO_3$ as a $CO_2$ sorbent precursor [22, 23]. Those studies have shown that $CaCO_3$ bio-derived materials exhibit sufficient $CO_2$ sorption capability. In some cases, these materials even displayed a higher performance than limestone. Nevertheless, in such reports, the experimental conditions employed were far from realistic, avoiding the harsh calcination conditions expected during calcination in the $CO_2$ capture application. To the best of our knowledge, neither eggshell nor snail shell have yet been considered in process simulations for the use of the CaL technology in $CO_2$ capture and energy storage applications aimed at assessing the techno-economic feasibility of this technology. For this purpose, it is of paramount importance to know beforehand the CaL multicycle performance of the material at realistic CaL conditions. As shown in previous works [24], in which the techno-economic assessment was carried out for other Ca-based sorbents, such as limestone, dolomite and steel slag, the present investigation is a first step to address the possible use of biogenic carbonates as CaO precursors for $CO_2$ capture and energy storage. Our main goal is, thus, to get information on the multicycle performance of these materials to be used in future works for process simulations, which are out of the scope of the present investigation

## 2. MATERIALS AND METHODS

The snail shells and eggshells used in this work were by-products supplied by local restaurants in Seville. The shells were thoroughly washed to remove any organic remains before testing. In this paper, we will refer to the washed samples as untreated. Besides, in order to assess the influence of different pretreatments on $CO_2$ capture performance, the samples were also treated using two different procedures: (i) One batch was ball-milled utilising a high-energy ball mill EMAX (Retsch), at 1200 rpm for 20 min. (ii) The second batch was calcined for four hours at 850 $^{o}$C in static air. For comparison, limestone powder Granicarb 0.1/0.8 provided by OMYA was employed. Figure 1 shows a photograph of the untreated shells and the limestone used in this work.


FIG. 1: Photograph of the untreated shells and the sample of limestone used in this work.

The multicycle calcination/carbonation cycles were carried out in a thermogravimetric analyser (TGA) Q5000IR from TA Instruments. This analyser is equipped with a highly sensitive balance (<0.1 µm) and a furnace heated through infrared halogen lamps, which allows high heating rates up to 300 $^{o}$C min$^{-1}$.

The experiments performed under $CO_2$ capture conditions (CaL-$CO_2$) comprised an initial calcination stage, heating the sample from room temperature up to 900 $^{o}$C under a 70 vol% $CO_2$/30 vol% air atmosphere at atmospheric pressure. The process was continued by successive carbonation/calcination cycles. The carbonation stages were carried out at 650 $^{o}$C for 5 minutes in an atmosphere of 15 % $CO_2$ and 85 % air by volume. The calcination stages were performed at 900 $^{o}$C in an atmosphere of 70 % $CO_2$ and 30 % air by volume. This $CO_2$ concentration has been used in previous works to mimic the conditions for $CO_2$ capture in CaL pilot plants [25, 26].

The multicycle carbonation/calcination tests in conditions that are relevant for thermochemical energy storage (CaL-TCES) were started with a decarbonation stage, heating the sample up to 750 $^{o}$C in an $N_2$ atmosphere. This first stage was followed by the carbonation/calcination cycles, consisting of 5-min long carbonation stages at 850 $^{o}$C in pure $CO_2$, and 5-min long calcination stages at 750 $^{o}$C under $N_2$. Figure 2 includes a scheme of the experimental protocols used for CaL-TCES and CaL-$CO_2$ experiments.

Since in practical applications the material circulates quickly between reactors at different temperatures, high heating and cooling rates (300 $^{o}$C min$^{-1}$) were used in our tests to consider realistic conditions [11]. This is especially relevant when calcination takes place under high $CO_2$ concentrations. In this situation, the transition time between carbonation and calcination must be minimised to avoid recarbonation of unreacted CaO when the sample overpasses the equilibrium temperature. The overshoot observed in the transition between carbonation and calcination (see Figure 5) is caused by fast carbonation of the unreacted CaO when $CO_2$ is introduced, and that occurs until the equilibrium temperature is exceeded. Above this equilibrium temperature decarbonation is initiated. The period during which recarbonation takes place is minimised by using a high heating rate in our tests. This would occur to some brief extent, in practice, when the partially carbonated particles are heated to the calcination temperature.

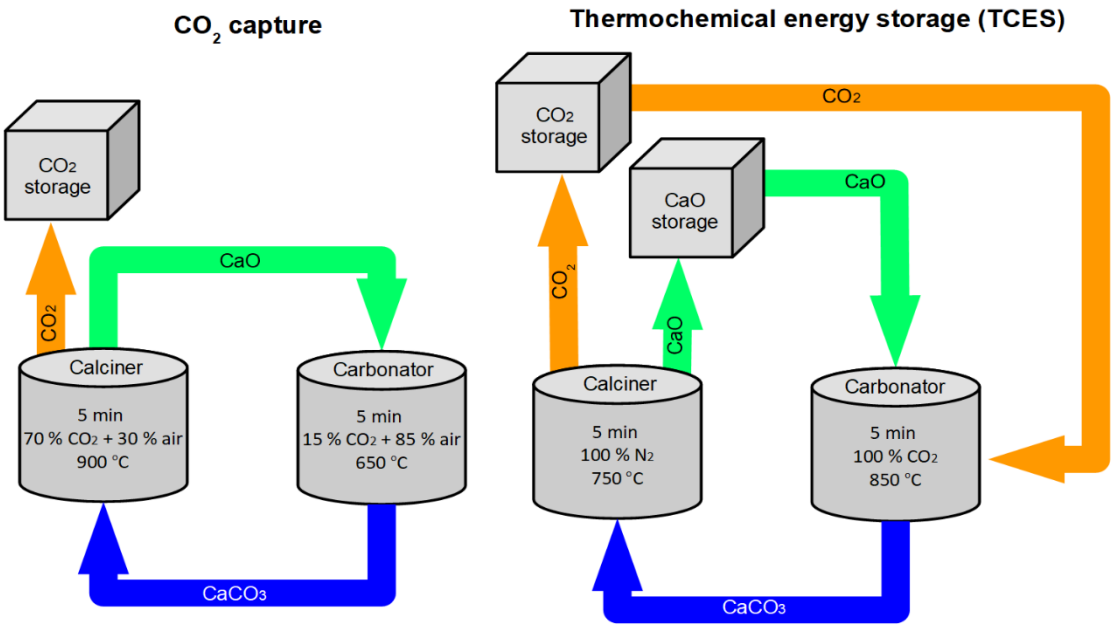


FIG. 2: Schematic illustration of the CaL process for $CO_2$ capture and TCES.

The microstructure of samples at different stages was studied by using a scanning electron microscopy (HITACHI S4800). Micrographs of the samples were taken before the cycles, as well as after one and ten calcination stages. Prior to the microscopy studies, the samples were coated with a thin layer of gold by means of an Emitech K550 Telstar sputter-coating machine (30 s, 30 mA). Figure 3 shows micrographs of the different samples used in this work, after the pretreatment but before the cycles.

X-ray diffractograms of the samples, before the multicycle tests, were acquired using a Rigaku Miniflex diffractometer working at 40 kV and 15 mA in the 2θ range from 10$^{o}$ to 60 $^{o}$. Figure 4 shows X-ray diffractograms corresponding to the different samples used in this work. Untreated and milled snail shell exhibit patterns that are characteristic of aragonite (00-005-0453), whereas the diffractograms of the untreated and milled eggshell correspond to calcite (01-072-1652). In the cases of precalcined snail shell and eggshell, both patterns are almost identical and are characteristic of portlandite (00-

004-0733, calcium hydroxide). $Ca(OH)_2$ is produced by the rapid hydroxylation of the CaO occurring after calcination when the material comes into contact with ambient air. A surface area analysis of the samples was performed by using a TriStar II (Micromeritics) instrument, in which the nitrogen adsorption-desorption isotherms were measured at 77 K. Total surface area was determined using the BET equation [27]. Prior to the analysis, the samples were degassed at 300 $^{o}$C for 2h. Since this analysis required, at least, a sample of 500 mg, in order to minimise the relative uncertainty of the measurement, a sample of 1 g was completely calcined under $N_2$ at 750 $^{o}$C for 1h, in an infrared heated tubular furnace. Table 1 shows the values of the surface area $S_{BET}$ obtained from the physisorption analysis. As can be seen, milling of the untreated samples yields a slight increase in the total surface area, whilst precalcination leads to a loss of surface area by sintering [7]. Data from X-ray fluorescence (XRF) analysis of the samples, as received, are collected in table 2.

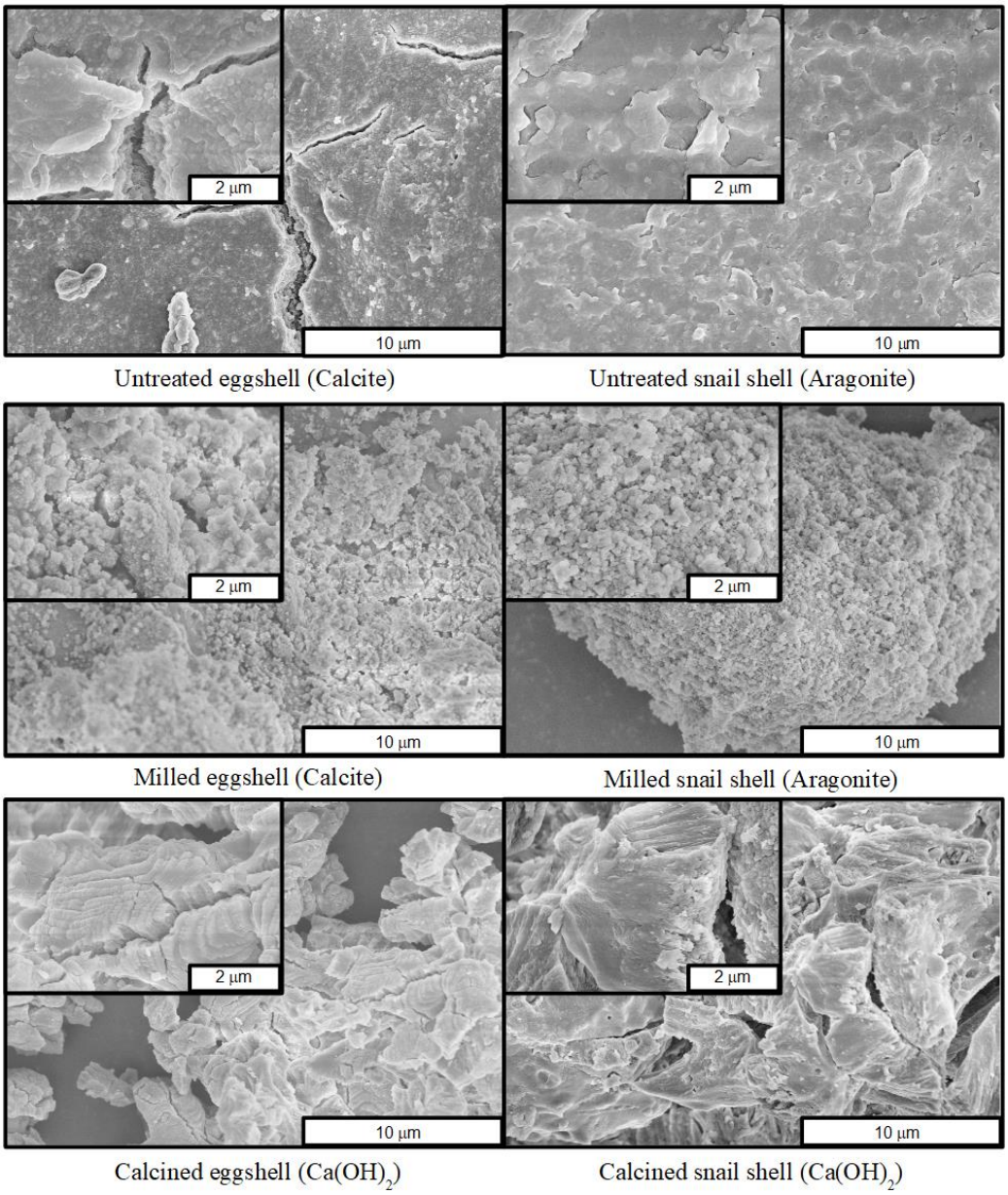

FIG 3: SEM micrographs of eggshell and snail shell samples tested in this work.

In the cases of the milled and calcined samples, particle size was around 20 microns. The experiments conducted with the untreated samples were performed using entire pieces of the shells of around 1 mm. Particle size has been proved to affect the results obtained in the CaL multicycle tests [28]. Enhancement of activity has been observed for the particles that are smaller than 15 microns, in the experiments conducted under CaL-TCES conditions using He for the calcination. The reason is that those small particles are more resilient to pore plugging [29].

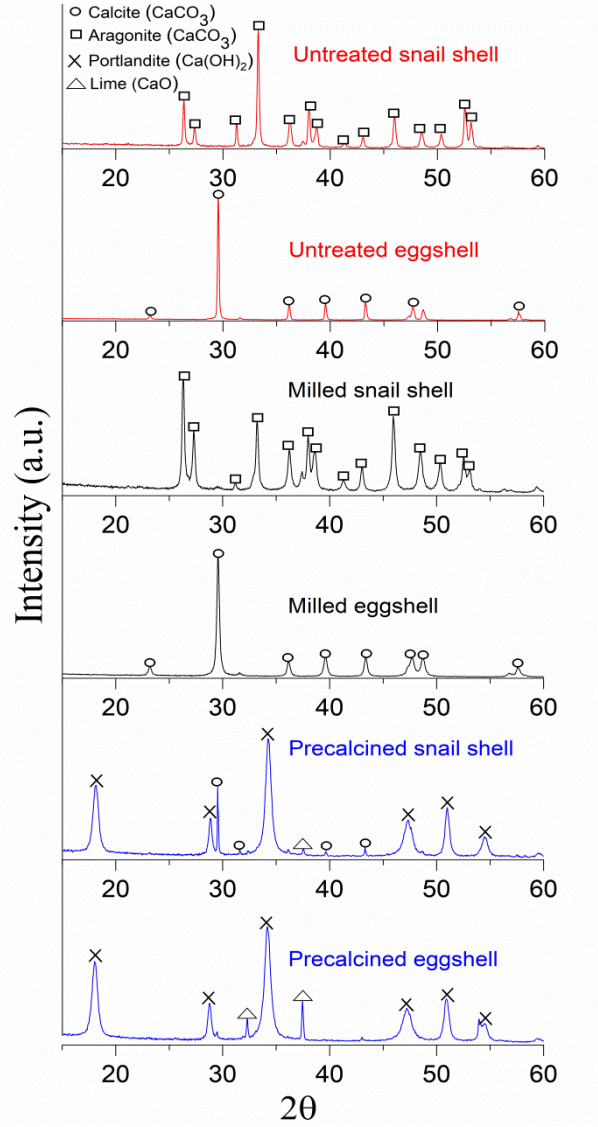


FIG 4: X-ray diffractograms of the different *CaO* precursors used in this work.

TABLE 1: Results of the physisorption analysis.

| $S_{BET}$ ($m^2$/g) | Untreated | Milled | Precalcined |
|---|---|---|---|
| Snail shell | 4.7 | 6.1 | 1.2 |
| Eggshell | 8.9 | 11.2 | 4.4 |
| Limestone Granicarb 0.1/0.8 | 0.4 | | |

TABLE 2: Results from XRF analysis of the samples as received. The last column corresponds to combustion losses (C.L.).

| | $SiO_2$(%) | $Al_2O_3$(%) | $Fe_2O_3$(%) | MgO(%) | CaO(%) | $Na_2O$(%) | $K_2O$(%) | C.L.(%) Combustion losses |
|---|---|---|---|---|---|---|---|---|
| Snail shell | 0.12 | 0.02 | 0.03 | 0.09 | 51.99 | 0.21 | 0.18 | 46.10 |
| Eggshell | 0.01 | 0.01 | 0.02 | 0.39 | 50.78 | 0.11 | 0.09 | 47 |

## 3. RESULTS AND DISCUSSION

### 3.1. CaL cycles in $CO_2$ capture conditions

Figure 5 shows the time evolution of the temperature and effective conversion for the untreated eggshell, corresponding to the first 15 cycles carried out in CaL-$CO_2$ conditions. Effective conversion is defined as the ratio of the mass of CaO converted to $CaCO_3$, to the total mass of the sample *m* (including inert solids if present) before carbonation proceeds:

$$X_{eff} = \frac{(m_{Carb}(t)-m)\cdot W_{CaO}}{m\cdot W_{CO_2}} \quad (1),$$

where $m_{Carb}$(t) is the sample mass at time t after carbonation is initiated, and $W_{CaO}$ and $W_{CO2}$ are the molar masses of CaO and $CO_2$, respectively. The effective conversion takes into account the existence of nonreactive compounds in the material by dividing the mass of CaO converted to the total sorbent mass, whereas the CaO conversion is obtained by dividing the mass of CaO converted to the initial mass of CaO. For practical purposes, the effective conversion, which is always smaller than the CaO conversion, is the most relevant parameter, since it allows this research to consider the presence of inert solids in the process simulations in order to estimate the energy consumption [24].

Effective conversion data, obtained for the different samples tested in our work under CaL-$CO_2$ conditions (at $\Delta$t=5 min from the beginning of carbonation in each cycle), are plotted in Figure 6. Effective conversion at the end of the first and the twentieth carbonation stages, as well as the residual effective conversion values estimated, are collected in Table 3. Data of conversion, as a function of the cycle number, usually fitted to the equation [30,31]

$$X_{eff,N} = X_r + \frac{X_{eff,1}}{k(N-1)+(1-X_r/X_{eff,1})^{-1}} \quad (2),$$

Where N represents the number of the cycle, k the deactivation rate constant, $X_{eff,1}$ the effective conversion at the first cycle, and $X_r$ the residual effective conversion. The residual effective conversion, which is estimated by fitting Eq. 2 to the data, represents the conversion towards which the conversion approaches, asymptotically, as the number of cycles is increased. In practice, effective conversion is very close to its residual value after hundreds of cycles.

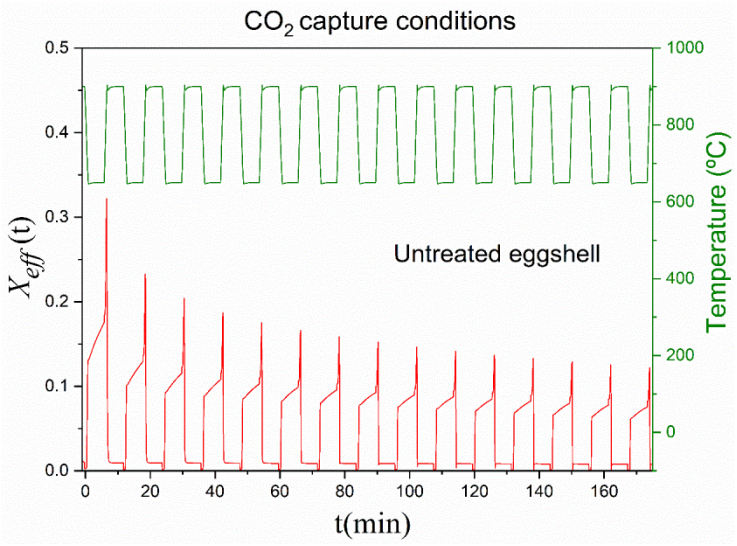


FIG 5: Time evolution of temperature and effective conversion for multicycle tests carried out using untreated eggshell.

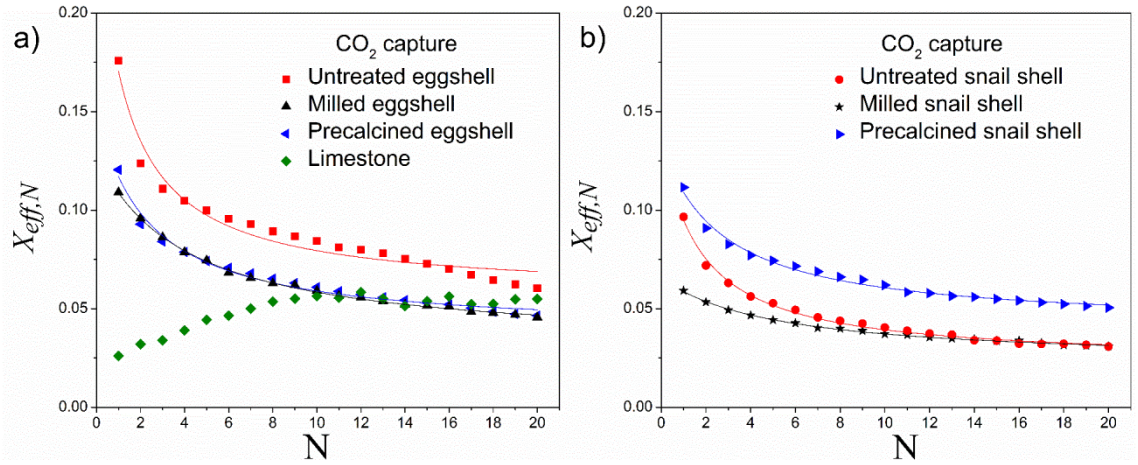


FIG 6: Effective conversion at the end of the 5-min carbonation stage, as a function of the cycle number, from tests carried out in CaL-$CO_2$ conditions. Lines represent the curves that best fit the data, according to Eq. 2. For the sake of clarity, the results have been shown in two separated graphs, a) and b). The correspondence between samples and symbols is given in the legend.

The sample that exhibits the best performance was untreated eggshell, whilst the worst corresponds to the milled snail shell. Previous studies with limestone and dolomite have shown the negative effect that milling might have on the effective

conversion of these samples, as the reduction in particle size and the introduction of defects in the crystalline structure promote solid-state diffusion and strongly enhance sintering [32]. The value of conversion obtained for limestone after 20 cycles is similar to that exhibited by biomineralised samples, or even lower when compared to the untreated eggshell. In real applications, the sorbents are subjected to hundreds of cycles. Thus residual conversion is the most important parameter to assess the sample's performance. Note that the residual conversion for untreated eggshell is equal to the conversion exhibited by limestone after 20 cycles.

Due to incomplete decarbonation in the first cycles, conversion values for limestone are below those obtained for the biomineralised samples during the first cycles. Previous works have already shown that the complete decarbonation of limestone and dolomite under $CO_2$ capture conditions cannot be attained at 900 $^{o}$C, as used in our tests in short residence times (up to 5 minutes), as required in practice [32]. This has been confirmed for the limestone sample used in the present work, as can be seen in Figure 7.

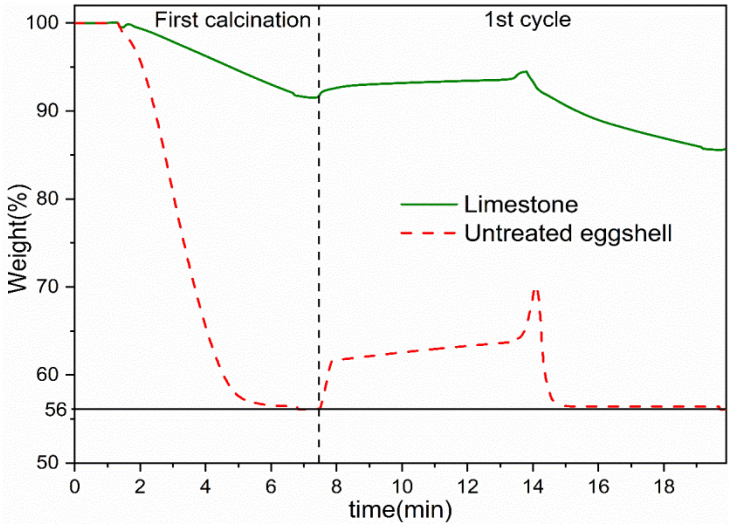


FIG 7: Thermograms during the first calcination and the first cycle obtained for limestone and untreated eggshell for tests carried out under $CO_2$ capture conditions. Calcination was carried out at 900$^{o}$C.

In the case of limestone, a minimum temperature of about 950 $^{o}$C is needed to achieve complete calcination in short residence times [5], while our work shows that full calcination is achieved for the biomineralised samples at just below 900$^{o}$C in less than 5 min. Thus, the use of biomineralised $CaCO_3$ would in practice allow for the saving of energy for the calcination.

Figure 8 shows micrographs of untreated eggshell and milled eggshell after one and ten cycles ending in the calcination. As can be clearly observed in the micrographs, the loss of porosity and surface area is markedly enhanced with the cycle number, leading, consequently, to a decrease of conversion due to sintering as shown by the data.

Previous works have pointed out the important role of the crystal structure on the performance of the sorbent for CaL-$CO_2$ tests [33]. Ca-based materials with a calcite

crystal structure typically exhibit better performance for $CO_2$ capture than those with an aragonite structure, which is consistent with our results [34, 35]. On the other hand, the presence of $Na_2O$ in some limestone samples has been reported to promote sintering [36], which is likely to occur also in the presence of $K_2O$. According to our XRF analysis (Table 2), both of the sintering promoting oxides are major impurities in the snail shell and eggshell, which may explain the relatively faster deactivation observed for both materials as compared to the limestone. Note also that deactivation is even more marked for the snail shell, with a higher $Na_2O$ and $K_2O$ content, as compared to the eggshell, which is consistent with this argument (Table 2).

TABLE 3: Effective conversion at the first and twentieth cycles and residual effective conversion for the samples tested under $CO_2$ capture conditions. Residual conversion values are obtained by fitting Eq. 2 to the data.

| $CO_2$ capture conditions | | | |
|---|---|---|---|
| Sample | $X_{eff,1}$ | $X_{eff,20}$ | $X_{eff,r}$ |
| Untreated snail shell | 0.097 | 0.030 | 0.023 |
| Untreated eggshell | 0.176 | 0.060 | 0.055 |
| Milled snail shell | 0.059 | 0.030 | 0.023 |
| Milled eggshell | 0.109 | 0.046 | 0.030 |
| Precalcined snail shell | 0.112 | 0.052 | 0.041 |
| Precalcined eggshell | 0.121 | 0.047 | 0.038 |
| Limestone | 0.026 | 0.055 | --- |

*** Calcination of limestone was incomplete at 900 $^{o}$C. Thus, Eq. 2 does not fit well to the data for estimating its residual conversion. The residual conversion of limestone typically given in the literature is around 0.07 [5].**

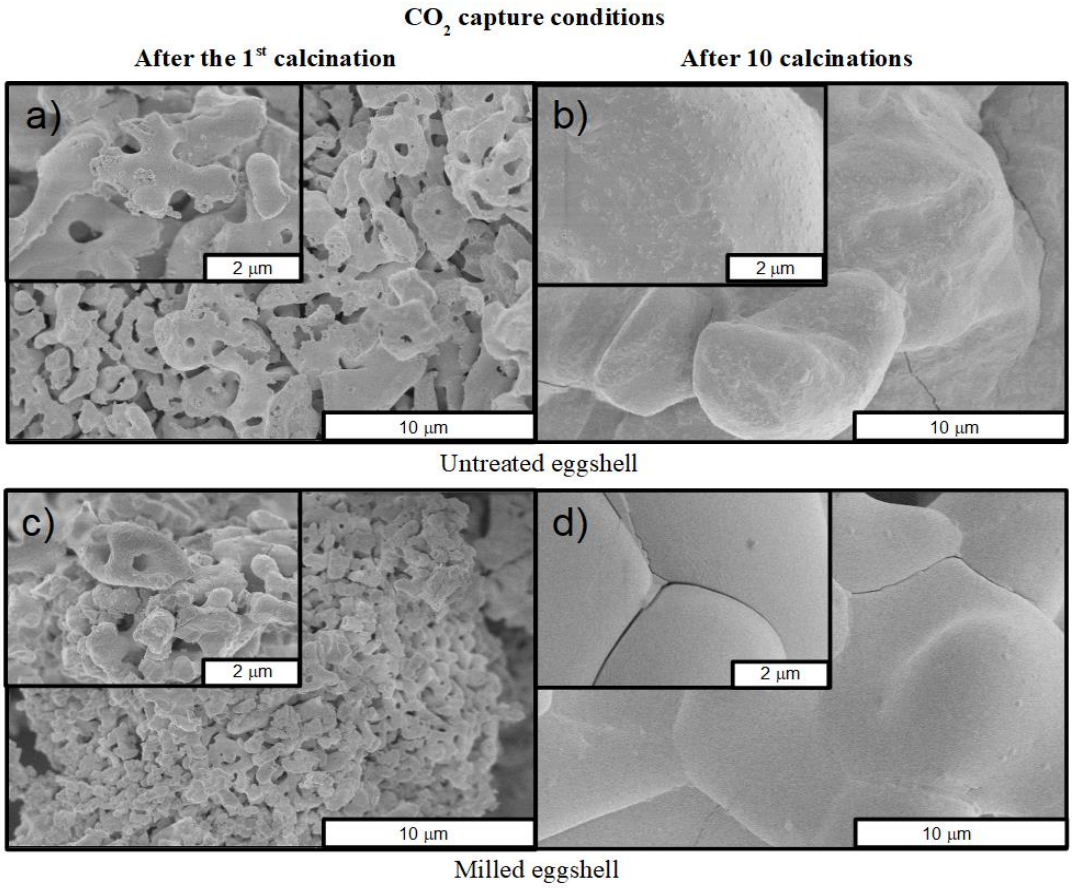


FIG 8: SEM micrographs of untreated eggshell and milled eggshell after one and ten CaL cycles (ending in calcination), carried out under $CO_2$ capture conditions. a) and b) SEM micrographs of Untreated eggshell after one and ten CaL cycles, respectively. c) and d) SEM micrographs of milled eggshell after one and ten CaL cycles, respectively.

### 3.2. CaL cycles under thermochemical energy storage conditions

In CaL-TCES tests, a relevant property is the energy per unit of mass released during the carbonation at the Nth-cycle, which is given by the expression $X_{eff,N} \cdot (\Delta H/W_{CaO})$, where $X_{eff,N}$ is the effective conversion at the end of the carbonation stage at the Nth-cycle and ΔH is the enthalpy of reaction (about 180 kJ/mol).

As an example, Figure 9 shows the time evolution of temperature and effective conversion corresponding to precalcined eggshell during the first 15 cycles carried out under TCES conditions. Effective conversion values obtained for the different samples tested in the CaL-TCES experiments are shown in Figure 10. Data for the eggshell and snail shell are presented separately for the sake of clarity. Values at the first and twentieth cycles are collected in Table 4. Equation 2 does not fit well to the data for estimating residual conversion values. The decay of conversion measured under TCES conditions do not conform to the exponential decay law observed for the tests carried out under $CO_2$ capture conditions. Thus, the value of conversion at the twentieth cycle was taken as a reference for comparison instead of the residual conversion, which is uncertain. The conversion attained by limestone under these experimental conditions

is similar to that exhibited by biomineralised $CaCO_3$ sources. Remarkably, as can be seen in Table 4, compared to some biomineralised samples, the conversion showed by limestone is lower after 20 cycles. Precalcined eggshell exhibited the best performance after 20 cycles, whilst the worst conversion was obtained for milled eggshell ($X_{eff,20}$ = 0.176). Limestone typically shows an effective conversion when cycled under TCES conditions of around 0.2 after 20 cycles depending on the particle size [28, 37–39], which is similar to the values obtained for the biomineralised $CaCO_3$ samples used in our work.

BET Surface area values obtained from the physisorption analysis are collected in table 1. The precalcined samples have the lowest values of $S_{BET}$ because of the heat pretreatment. Consequently, they exhibit low conversions during the first cycles, albeit conversion decays at lower rates in the following cycles. In contrast, milled samples display a higher surface area, and, therefore, relatively high conversions during the first cycles but also accelerated decay rates.

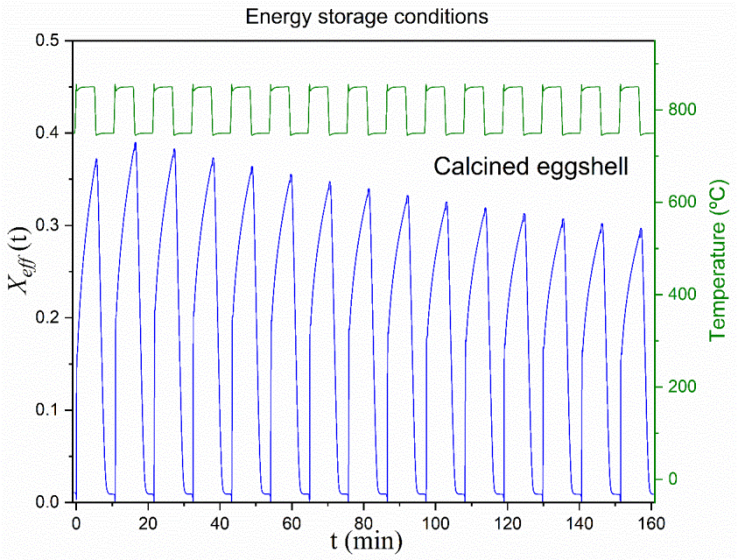


FIG 9: Time evolution of temperature and effective conversion obtained in multicycle tests carried out using precalcined eggshell under TCES conditions.

Precalcined eggshell (Figure 10a) shows a slightly higher conversion in the second cycle as compared to the first cycle. As previously reported [40], such reactivation has been observed in materials subjected to heat pretreatment prior to the cycles. The first carbonation of such strongly sintered materials is mainly driven by solid-state diffusion since the surface area available for fast carbonation is significantly reduced. The subsequent calcination leads to the formation of a porous CaO skeleton with an increased conversion in the second cycle and enhanced resilience to sintering induced decay. Besides, reactivation is not observed for the precalcined snail shell. The apparent reactivation shown by the untreated eggshell is just due to the incomplete decarbonation in the first calcination, thereby presenting a conversion at the second cycle that is higher than at the first cycle.

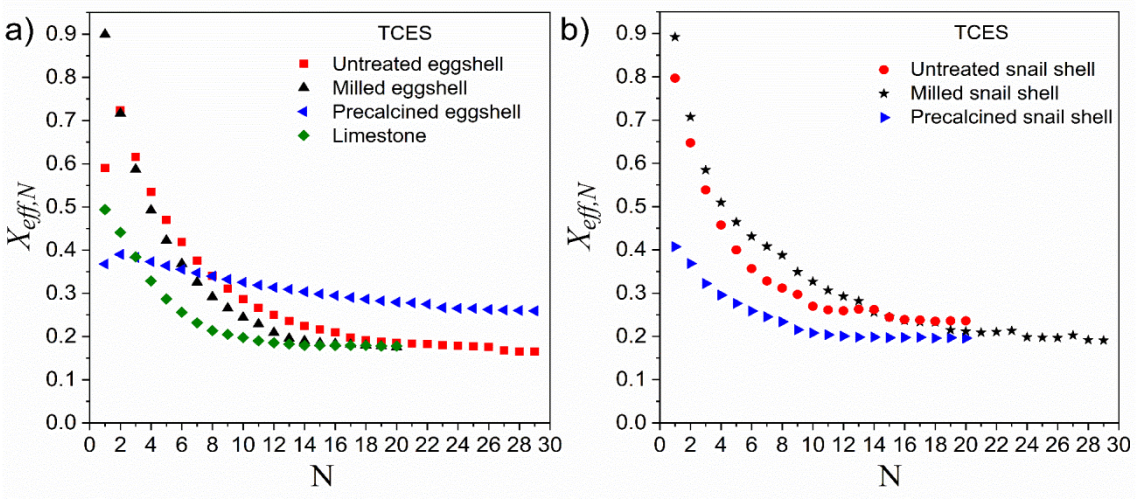


FIG 10: Effective conversion measured at the end of the carbonation stage as a function of the number of CaL cycles for samples tested under TCES conditions. For the sake of clarity, the results for the eggshell and snail shell have been separated in two graphs.

TABLE 4: Effective conversion measured at the end of the carbonation stage for the first and twentieth cycles and residual conversion for the samples tested under TCES conditions. Residual conversion values are obtained by fitting Eq. 2 to the experimental data.

| TCES conditions | | |
|---|---|---|
| Sample | $X_{eff,1}$ | $X_{eff,20}$ |
| Untreated snail shell | 0.797 | 0.236 |
| Untreated eggshell | 0.859 | 0.185 |
| Milled snail shell | 0.892 | 0.212 |
| Milled eggshell | 0.899 | 0.176 |
| Precalcined snail shell | 0.407 | 0.196 |
| Precalcined eggshell | 0.368 | 0.279 |
| Limestone | 0.689 | 0.207 |

Figure 11 shows the time evolution of an effective conversion during a typical carbonation/calcination cycle. Two distinct carbonation phases can be identified; a fast carbonation phase controlled by the reaction kinetics occurring at the surface of the particles, followed by a second phase where carbonation is controlled by the solid-state diffusion of $CO_2$ across the $CaCO_3$ layer built upon the CaO surface during the first reaction-controlled fast phase [41, 42]. As it can be observed in Figure 11, conversion for limestone derived CaO takes place almost exclusively during the fast reaction-controlled phase. On the other hand, in the case of the CaO obtained from biomineralised $CaCO_3$ samples, the extent of carbonation during the diffusion-controlled phase is significantly enhanced. For instance, in the case of a milled snail shell, the contribution of diffusion-controlled carbonation amounts to about 26 % of the overall conversion, as compared to only 8% in the case of limestone-derived CaO. For the precalcined eggshell, diffusion is even more relevant as the mass gained at this stage represents approximately 56 % of the total mass gained. The importance of diffusive carbonation for CaO, derived from biomineralised materials, has been

pointed out in previous works, albeit for tests carried out under $CO_2$ capture experimental conditions [19]. Another important difference between the behaviours displayed by limestone and biomineralised materials lies in the calcination rate. As seen in Figure 11, the time required for complete calcination is shorter for biomineralised $CaCO_3$ samples as compared to limestone. Indeed, calcination of limestone was incomplete during the first cycle. This feature might be relevant for practical purposes since calcination could be achieved in shorter residence times, thereby avoiding excessive CaO sintering, which could eventually improve the process efficiency [24]. Faster calcination kinetics were also observed in our work for the biomineralised materials in the tests performed under $CO_2$ capture conditions, while, in these tests, limestone did not calcine completely in the 5-min calcination stages.

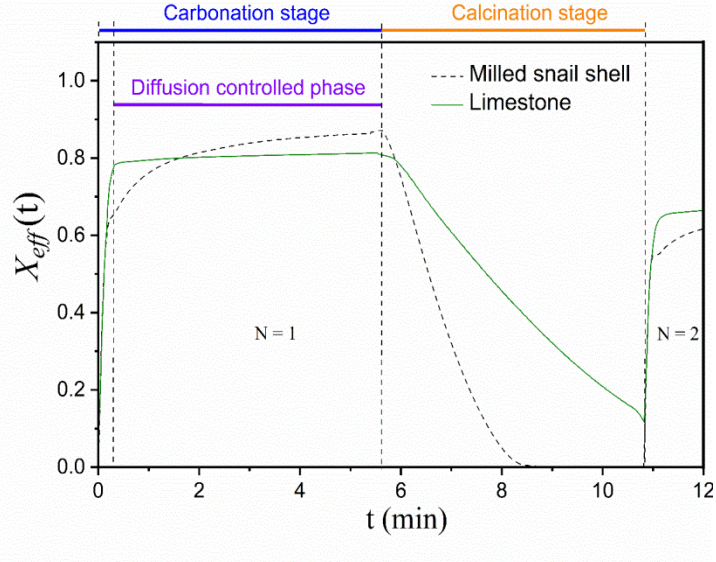


FIG 11: Time evolution of effective conversion during the first carbonation stage and the subsequent calcination for tests performed using snail shell and limestone under TCES conditions.

Figure 12 shows representative micrographs of samples after the first and tenth calcination. As for the samples tested under $CO_2$ capture conditions, a significant loss of porosity after ten cycles is apparent from these pictures. However, a higher porosity is observed when compared to samples tested under $CO_2$ capture conditions. The higher porosity is a consequence of the milder calcination conditions (lower temperature and inert atmosphere). As reported in the literature, calcination at high temperature in a $CO_2$ enriched environment strongly promotes sintering, which leads to a significant decrease in the surface area available for carbonation [7].

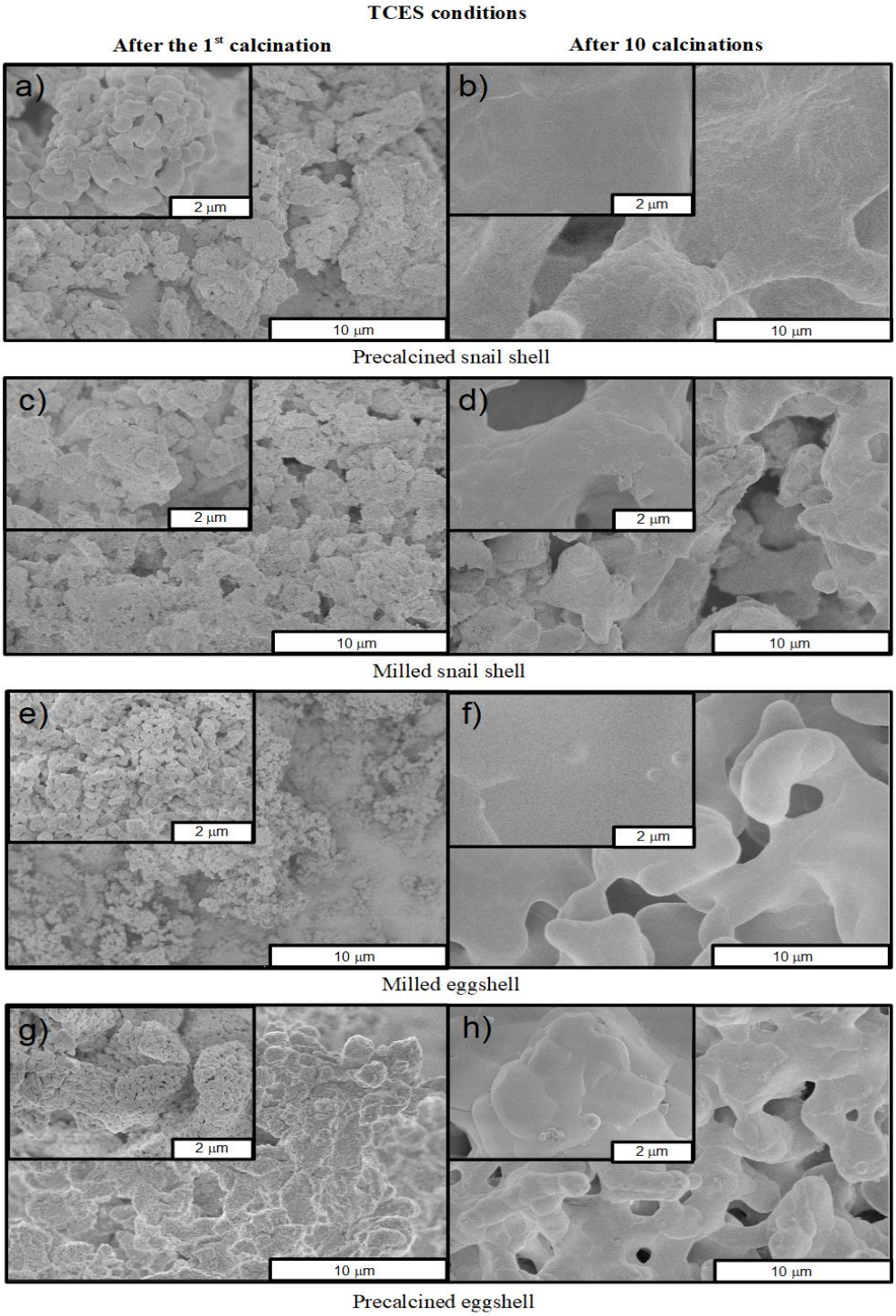


FIG 12: SEM micrographs of precalcined snail shell and milled snail shell after one and ten calcinations for CaL cycles carried out under TCES conditions. a) and b) Precalcined snail shell after one and ten CaL cycles, respectively. c) and d) Milled snail shell after one and ten CaL cycles, respectively. e) and f) Milled eggshell after one and ten CaL cycles, respectively. g) and h) Precalcined eggshell after one and ten CaL cycles, respectively.

### 3.3. Conversion at the fast reaction-controlled and the diffusion-controlled phases

Determining the relative contributions of the fast reaction-controlled and slower diffusion-controlled phases to the overall carbonation is relevant for practical

purposes, since it may help in optimising the residence time of the solids in the carbonator in order to enhance the process efficiency [24].

Figure 13a) and b) show, respectively, the extent of conversion attained during the fast reaction-controlled phase ($X^{f}_{eff,N}$) and the diffusion-controlled phase ($X^{d}_{eff,N}$). Data correspond to tests carried out under both $CO_2$ capture and TCES conditions. For the sake of clarity, only a representative selection of samples is compared. For the CaL-TCES tests, there is a remarkable difference between the precalcined samples, which show a similar conversion in both stages regardless of the cycle number, and the rest of the samples. For non-thermally pretreated biomineralised materials, carbonation takes place mostly during the fast reaction-controlled phase for the first cycles. As the material sinters progressively during the subsequent cycles, the difference in conversion for the fast and diffusion phases decreases. In the case of $CO_2$ capture conditions, the extent of conversion occurs mainly in the fast-reaction phase for all cases. However, the importance of conversion in the fast-reaction phase is especially relevant for untreated samples.

The ratio between conversions at both phases $r = X^{f}_{eff,N} / X^{d}_{eff,N}$ is plotted in Figure 13c) and d) for the tests carried out under $CO_2$ capture and TCES conditions. Note that for both conditions, this ratio shows an increasing trend with the cycle number, which is consistent with results reported for limestone in a previous study [43]. The same work also demonstrated that heat pretreatment promotes the values of r during the first cycles. This can be clearly observed also in Figure 13d, where the values of r for the precalcined samples are seen to be the highest during the first cycles carried out under TCES conditions. As conversion during the diffusion-controlled phase is approximately constant with the cycle number for all the samples, and for the TCES and $CO_2$ capture conditions, it may be inferred that deactivation is mainly driven by a loss of conversion in the fast reaction-controlled stage.

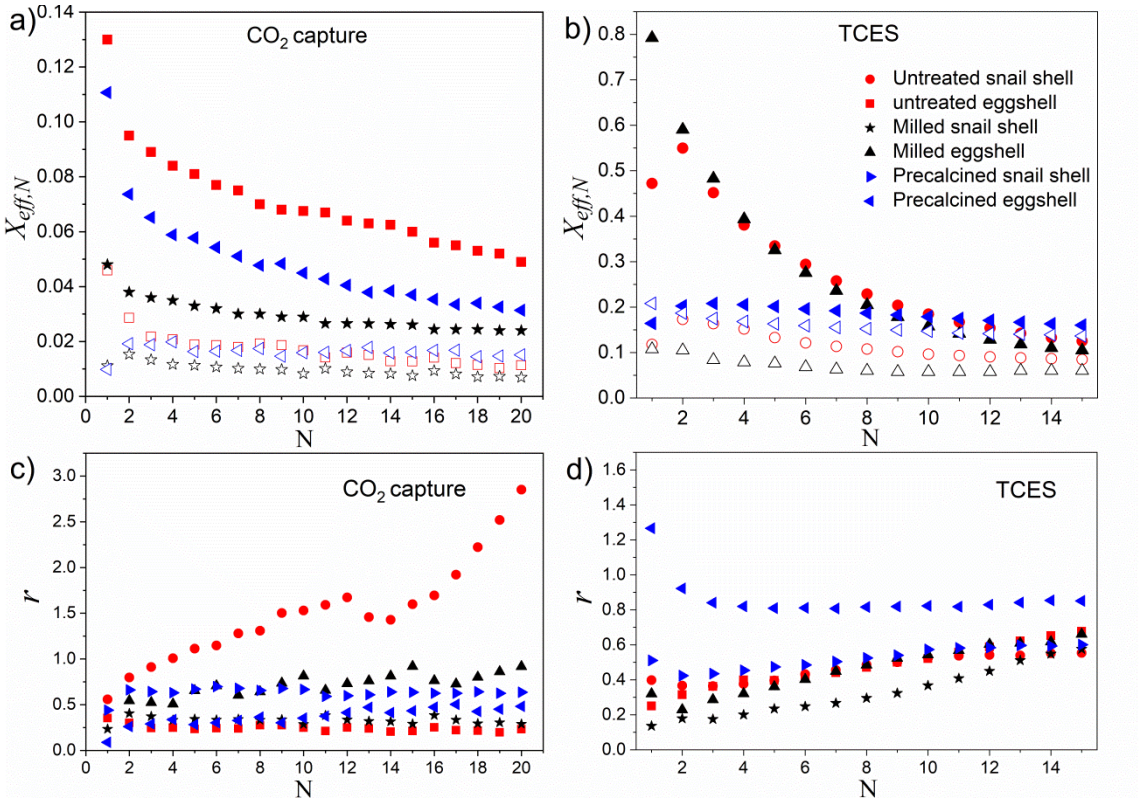


FIG 13: a) and b) Effective conversion at the fast reaction controlled (solid symbols) and slower diffusion-controlled phases (open symbols) for tests carried out under $CO_2$ capture and TCES conditions, respectively. For reasons of clarity, not all of the data have been plotted. c) and d) Ratio of conversion at the diffusion-controlled stage to the conversion during the fast phase as a function of the cycle number for tests carried out under $CO_2$ capture and TCES conditions, respectively. The legend in b) is common to all graphs.

## 4. CONCLUSIONS

In this work, we have explored the multicycle performance of snail shell and eggshell for TCES and $CO_2$ capture by means of the CaL process. These waste materials were tested without any pretreatment and after being subjected to mechanical and thermal pretreatments as applied in previous works for limestone. Remarkably, the sample that exhibited the best performance under $CO_2$ capture conditions was untreated eggshell, which is advantageous from an economic perspective as they can be directly used, as received from the food industry, without any thermal or mechanical pretreatment.

Importantly, the temperature needed for achieving full calcination of the biomineralised $CaCO_3$ samples at short residence times under $CO_2$ capture conditions is lower than those typically required for limestone, which would result in energy savings for calcination. Moreover, for biomineralised samples, conversion values measured under TCES conditions are similar, even higher in several cases, to those obtained for limestone. Compared to limestone, the shells exhibited better performance for carbonation during the diffusion-controlled stage, while complete decarbonation was achieved in shorter times. Furthermore, taking into account their enhanced mechanical strength (reported in previous works) and low cost, it may be

argued that snail shell and eggshell are feasible candidates to be employed as CaO precursors for TCES and $CO_2$ capture applications, which provides a useful outlet for these wastes.

**Acknowledgements**

This work was supported by Spanish Goverment Agency Ministerio de Economía y Competitividad (contracts No. CTQ2017-83602-C2-1-R and -2-R). PSJ is supported by a Ramón y Cajal Grant provided by the Ministerio de Economía y Competitividad. We also acknowledge the funding received by the European Union's Horizon 2020 research and innovation programme under grant agreement No 727348, project SOCRATCES.

**References**

[1] The Intergovernmental Panel on Climate Change; **2020**. https://www.ipcc.ch/sr15/

[2] Abanades, J. C.; Anthony, E. J.; Lu, D. Y.; Salvador, C.; Alvarez, D. Capture of $CO_2$ from combustion gases in a fluidised bed of CaO. *AIChE Journal*. **2004**, 50 (7), 1614-1622.

[3] Blamey, J.; Anthony, E. J.; Wang, J.; Fennell, P. S. The calcium looping cycle for large-scale $CO_2$ capture. *Prog. Energy Combust. Sci.* **2010**, 36(2), 260-279.

[4] Hanak, D. P.; Anthony, E. J.; Manovic, V. Demonstration of steady state $CO_2$ capture in a 1.7 MWth calcium looping pilot. *Int. J. Greenhouse Gas Control*. **2013**, 18, 237-245.

[5] Perejón, A.; Romeo, L. M.; Lara, Y.; Lisbon, P.; Martínez, A.; Valverde, J. M. The Calcium Looping technology for $CO_2$ capture: On the important roles of energy integration and sorbent behavior. *Applied Energy*. **2016**, 162, 787-807.

[6] Boot-Handford, M.E.; Abanades, J.C.; Anthony E. J.; Blunt, M.J.; Brandani, S.; Mac Dowell, N.; Fernández, J. R.; Ferrari, M.; Gross, R.; Hallett, J. P.; Haszeldine, R. S.; Heptonstall, P.; Lyngfelt, A.; Makuch, Z.; Mangano, E.; Porter, R.; Pourkashanian, M.; Rochelle G. T.; Shah, N.; Yao, J.G.; Fennell, P. S. Carbon capture and storage update. *Energy & Environmental Science*. **2014**. 7 (1), 130-189.

[7] Borgwardt, R. H. Sintering of nascent calcium oxide. *Chemical Engineering Science*. **1989**, 44(1), 53-60.

[8] Sanchez-Jimenez, P. E.; Valverde, J. M.; Perez-Maqueda, L. A. Multicyclic conversion of limestone at Ca-looping conditions: The role of solid-sate diffusion controlled carbonation. *Fuel*. **2014**. 127, 131-140.

[9] Valverde, J. M.; Sánchez-Jiménez, P. E.; Perejón, A.; Pérez-Maqueda, L. A. Constant rate of thermal analysis for enhancing the long-term $CO_2$ capture of CaO at ca-looping conditions. *Appl. Energy*. **2013**, 108, 108-120.

[10] Dean, C.C.; Blamey, J.; Flori, N.H.; Al-Jeboori, M.J.; Fennell, P.S. The calcium looping cycle for $CO_2$ capture from power generation, cement manufacture and hydrogen production. *Chemical Engineering Research and Design.* **2011**. 89, 836-865.

[11] Chacartegui, R.; Alovisio, A.; Ortiz, C.; Valverde, J. M.; Verda, V.; Becerra, J. A. Thermochemical energy storage of concentrated solar power by integration of the calcium looping process and a $CO_2$ power cycle. *Applied Energy*, **2016**, 173, 589-605.

[12] Prieto, C.; Cooper, P.; Fernández, A. I.; Cabeza, L. F. Thermochemical energy storage for concentrated solar power plants. *Renew. Sustain. Energy. Rev*., **2016**, 60, 909-929.

[13] Flamant, G.; Hernandez, D.; Bonet, C.; Traverse, J. P. Experimental aspects of the thermochemical conversion of solar energy; decarbonation of $CaCO_3$. *Sol. Energy.,* **1980**, 24, 385-395.

[14] Benítez-Guerrero, M.; Valverde, J. M.; Sánchez-Jiménez, P. E.; Perejón, A.; Pérez-Maqueda, L. A. Multicycle activity of natural $CaCO_3$ minerals for thermochemical energy storage in Concentrated Solar Power plants. *Solar Energy*, **2017**, 153, 188-199.

[15] Erans, M.; Manovic, E.; Anthony, E. J. Calcium looping sorbents for $CO_2$ capture. *Applied Energy,* **2016***,* 180, 722-742.

[16] Romeo, L. M.; Lara, Y.; Lisbona, P.; Martínez, A. Economical assesment of competitive enhanced limestones for $CO_2$ capture cycles in power plants. *Fuel Process Technol*., **2009**, 90(6), 803-11.

[17] Manovic, V.; Anthony, E. J. Thermal Activation of CaO-Based Sorbent and Self-Reactivation during $CO_2$ Capture Looping Cycles. *Environ. Sci. Technol*, **2008**, 42, 4170–4174.

[18] SOCRATCES (SOlar Calcium-looping integRAtion for Thermo-Chemical Energy Storage). **2019**. https://cordis.europa.eu/project/rcn/212577/factsheet/en.

[19] Castilho, S.; Kiennemann, A.; Costa-Pereira, M. F.; Soares-Dias, A. P. Sorbents for $CO_2$ capture from biogenesis calcium wastes. *Chem. Eng. J,* **2013**, 226, 146-153.

[20] Sacia, E. R.; Rankumar, S.; Phalak, N.; Liang-Shih, F. Synthesis and regeneration of sustainable CaO sorbents from chicken eggshells for enhanced carbon dioxide capture. ACS Sustainable. *Chem. Eng.,* **2013**, 1, 903-909.

[21] Food and Agriculture Organization of the United nations. **2019**. http://www.fao.org

[22] Ives, M.; Mundy, R. C.; Fennell, P. S.; Davidson, J. F.; Dennis, J. S. Hayhurst, A. N. Comparison of Different Natural Sorbents for Removing $CO_2$ from Combustion Gases, as Studied
in a Bench-Scale Fluidised Bed. *Energy Fuels*, **2008**, 22(6), 3852-3857.

[23] Li, Y. J.; Zhao, C. S.; Chen, H. C.; Duan, L. B.; Chen, X. P. $CO_2$ Capture Behavior of Shell during Calcination/Carbonation Cycles. *Chem. Eng. Technol*, **2009**, 32(8), 1176-1182.

[24] Ortiz, C.; Valverde, J. M.; Chacartegui, R. Energy Consumption for $CO_2$ Capture by means of the Calcium Looping Process: A Comparative Analysis using Limestone, Dolomite, and Steel Slag. *Energy Technology***, 2016** 4(10), 1317-1327.

[25] Sánchez-Jiménez, P. E.; Valverde, J. M.; Pérez-Maqueda, L. A. Multicyclic conversion of limestone at Ca-looping conditions: The role of solid-sate diffusion controlled carbonation. *Fuel,* **2014**, 127, 131-140.

[26] Valverde, J. M.; Sánchez-Jiménez, P. E.; Perejón, A.; Pérez-Maqueda, L. A. Role of looping calcination conditions on self-reactivation of thermally pretreated $CO_2$ sorbents based on CaO. *Energy and Fuels*, **2013,** 27, 3373- 3384.

[27] Brenauer, S.; Emmett, P. H.; Teller, E. Adsorption of gases in multimolecular layers. *J. Am. Chem. Soc*., **1938**, 60, 309-319.

[28] Durán-Martín, J. D.; Sánchez-Jimeneza, P. E.; Valverde, J. M.; Perejón, A.; Arcenegui-Troya, J.; García-Triñanes, P.; Pérez-Maqueda, L. A. Role of Particle Size on the Multicycle Calcium Looping Activity of Lime-stone for Thermochemical Energy Storage. *Journal of Advanced Research*. **2020**, 22, 67-76.

[29] Benitez-Guerrero, M.; Sarrion, B.; Perejon, A.; Sanchez-Jimenez, P. E.; Perez-Maqueda, L. A.; Valverde, J. M. Large-scale high-temperature solar energy storage using natural minerals. *Solar Energy Materials and Solar Cells.* **2017**, 168, 14-21.

[30] Grasa, G.S.; Abanades, J. C. $CO_2$ capture capacity of CaO in long series of carbonation/calcination cycles. *Ind Eng Chem Res*, 2006, 45 (26), 8846-8851.

[31] Valverde, J. M.; Sánchez-Jiménez, P. E.; Perejón, A.; Pérez-Maqueda, L. A. $CO_2$ multicyclic capture of pretreated/doped CaO in the Ca-Looping process. Theory and experiments. *Phys.Chem.Chem*. *Phys.,* **2013**, 13, 11775-11793.

[32] Sánchez-Jiménez, P. E.; Valverde, J. M.; Perejón, A.; de la Calle, A.; Medina, S.; Pérez-Maqueda, L. A. Influence of Ball Milling on CaO Crystal Growth During Limestone and Dolomite Calcination: Effect on $CO_2$ Capture at Calcium Looping Conditions. *Cryst. Growth Des***., 2016**, 16, 7025-7036.

[33] Valverde, J. M.; Sánchez-Jiménez, P. E.; Pérez-Maqueda, L. A.; Quintanilla, M. A. S.; Pérez-Vaquero, J. Role of crystal structure on $CO_2$ capture by limestone derived CaO subjected to carbonation/recarbonation/calcination cycles at Ca-Looping conditions. *Applied Energy*, **2014**, 125, 264-275.

[34] Alvarez, D.; Peña, M.; Borrego, A. G. Behavior of Different Calcium-Based Sorbents in a Calcination/Carbonation Cycle for $CO_2$ Capture*. Energy and Fuels***, 2007** 21, 1534-1542.

[35] Olivares-Marín, M.; Cuerda-Correa, E. M.; Nieto-Sánchez, A.; García, S.; Pevida, C.; Román, S. Influence of morphology, porosity and crystal structure of $CaCO_3$ precursors on the $CO_2$ capture performance of CaO-derived sorbents. *Chem. Eng. J*., **2013**, 217, 71-81.

[36] Manovic, V.; Anthony, E. J.; Grasa, G.; Abanades, J. C. $CO_2$ Looping Cycle Performance of a High-Purity Limestone after Thermal Activation/Doping. *Energy Fuels*, **2008**, 22, 3258–3264.

[37] Benitez-Guerrero, M.; Valverde, J. M.; Sanchez-Jimenez, P. E.; Perejón, A.; Pérez-Maqueda,
L. A. Calcium-Looping performance of mechanically modified $Al_2O_3$-CaO composites for energy storage and $CO_2$ capture. *Chem. Eng. J***., 2018.** 334, 2343-2355.

[38] Carrillo, A. J.; González-Aguilar, J.; Romero, M.; Coronado, J. M. Solar Energy on Demand: A Review on High Temperature Thermochemical Heat Storage Systems and Materials*. Chem. Rev*., **2019**, 119, 4777-4816.

[39] Alonso, M.; Arias, B.; Fernández, J. R.; Bughin, O.; Abanades, C. Measuring attrition properties of calcium looping materials in a 30 kW pilot plant*. Powder Technology***, 2018**, 336, 273-281.

[40] Valverde, J. M.; Sánchez-Jiménez, P. E.; Perejón, A.; Pérez-Maqueda, L. A. Role of Looping Calcination Conditions on Self-Reactivation of Thermally Pretreated $CO_2$ Sorbents Based on CaO. *Energy Fuels*, **2013**, 27(6), 3373-3384.

[41] Barker, R. Reversibility of the reaction $CaCO_3$ = CaO + $CO_2$. *J. Appl. Chem. Biotechnol*, **1973**, 23, 733-742.

[42] Abanades, J. C.; Alvarez, D. Conversion Limits in the Reaction of $CO_2$ with Lime. *Energy & Fuels*. **2003**, 17, 308-315

[43] Sánchez-Jiménez, P. E.; Valverde, J. M.; Pérez-Maqueda, L. A. Multicyclic conversion of limestone at Ca-looping conditions: The role of solid-state diffusion controlled carbonation. *Fuel*, **2014** 127, 131-140.

[44] Currey, J. D.; The design of mineralised hard tissues for their mechanical functions. The *Journal of Experimental Biology*, **1999**, 202(23), 3285–3294.

[45] Lu, D. Y.; Hughes, R. W.; Anthony, E. J. ``Ca-based sorbent looping combustion for $CO_2$ capture in pilot-scale dual fluidised beds". *Fuel Processing Technology*, **2008**, 89(12), 1386–1395.